A Shock Tube Study of the $OH + OH \rightarrow H_2O + O$ Reaction

MARGARET S. WOOLDRIDGE, RONALD K. HANSON, and CRAIG T. BOWMAN

High Temperature Gasdynamics Laboratory, Department of Mechanical Engineering, Stanford University, Stanford, California 94305

Abstract

The rate coefficient for the reaction

(1) $$OH + OH \longrightarrow H_2O + O$$

has been determined in mixtures of nitric acid (HNO_3) and argon in incident shock wave experiments. Quantitative OH time-histories were obtained by cw narrow-linewidth uv laser absorption of the $R_1(5)$ line of the $A^2\Sigma^+ \leftarrow X^2\Pi_i(0,0)$ transition at 32606.56 cm^{-1} (vacuum). The experiments were conducted over the temperature range 1050–2380 K and the pressure range 0.18–0.60 atm. The second-order rate coefficient was determined to be

$$k_1 = 9.40 \times 10^{-5}\, T^{4.77} \exp(+4570/T\ [\mathrm{K}])\ [\mathrm{cm^3\ mol^{-1}\ s^{-1}}]$$

with overall uncertainties of +11%, −16% at high temperatures and +25%, −22% at low temperatures. By incorporating data from previous investigations in the temperature range 298–578 K, the following expression is determined for the temperature range 298–2380 K

$$k_1 = 3.57 \times 10^{4}\, T^{2.40} \exp(+1063/T\ [\mathrm{K}])\ [\mathrm{cm^3\ mol^{-1}\ s^{-1}}].$$

Introduction

The bimolecular reaction

(1) $$OH + OH \longrightarrow H_2O + O \qquad \Delta H^\circ_{298} = -16.9\ \mathrm{kcal/mol}$$

plays a key role in detailed kinetic modeling of combustion processes, including calculation of laminar flame speeds and species profiles in flames [1]. Due to the strong non-Arrhenius behavior of reaction (1), it is critical to have an accurate determination of the rate coefficient over an extended temperature range. Unfortunately, previous measurements of the rate coefficient at high temperatures display significant scatter.

This investigation seeks to provide an improved, direct determination of $OH + OH \rightarrow$ products. The products are assumed to be $H_2O + O$, since reaction (1) is energetically- and collisionally-favored over the other possible channels:

$$\begin{aligned} OH + OH &\longrightarrow HO_2 + H & \Delta H^\circ_{298} &= 36.0\ \mathrm{kcal/mol} \\ OH + OH &\longrightarrow H_2 + O_2 & \Delta H^\circ_{298} &= -18.6\ \mathrm{kcal/mol} \\ OH + OH + M &\longrightarrow H_2O_2 + M & \Delta H^\circ_{298} &= -51.2\ \mathrm{kcal/mol} \end{aligned}$$

Pyrolysis of nitric acid, HNO_3, behind incident shock waves is used as the source of OH radicals. The nitric acid rapidly decomposes via

(2) $$HNO_3 + M \longrightarrow OH + NO_2 + M$$

International Journal of Chemical Kinetics, Vol. 26, 389–401 (1994)

CCC 0538-8066/94/040389-13

Subsequently, the OH concentration profile is dominated by reaction (1). The OH is monitored by cw narrow-linewidth uv laser absorption of the $R_1(5)$ line of the $A^2\sum^+ \leftarrow X^2\prod_i (0,0)$ OH transition at 32606.56 cm^{-1} (vacuum). The direct, quantitative measurement of OH allows an accurate determination of the rate coefficient for reaction (1).

Experimental Details

A schematic diagram of the experimental facility is shown in Figure 1. All experiments were conducted behind incident shock waves in a 15.24 cm diameter, stainless steel, pressure-driven shock tube with a 2.3 m long driver section and a 10.5 m long driven section. Prior to each experiment, the driven section was evacuated to ca. 5×10^{-6} torr; the subsequent leak–plus–outgassing rate was ca. 20×10^{-6} torr/min. Shock speeds were measured using four platinum thin-film gauges equipped with signal amplifiers that triggered three time-interval counters. Shock wave attenuation was typically 1–2% per meter. All post-shock conditions were calculated using one-dimensional shock wave relations, assuming vibrational equilibrium and frozen chemistry. The calculation inputs were the initial test gas temperature, pressure, and composition, and the shock speed at the measurement position. Helium was used as the driver gas for all experiments.

The gases employed were Matheson Purity argon (99.9995%) and commercial grade helium (Liquid Carbonic, 99.9% minimum purity). The nitric acid was purchased

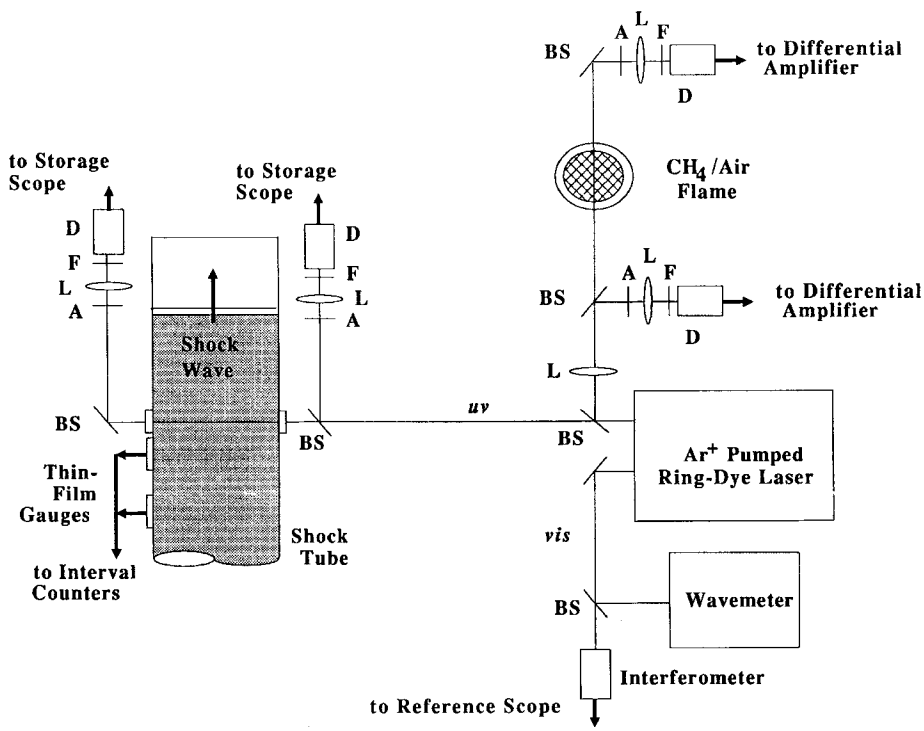

Figure 1. Experimental arrangement: solid lines, optical paths and bold lines, electrical paths. (A) aperture; (F) filter; (L) lens; (BS) beam-splitter; and (D) detector.

in 90% aqueous solution and subsequently dehydrated using a technique described by Stern, Mullhaupt, and Kay [2]. The dehydration process consisted of mixing one volume of nitric acid with two volumes of sulfuric acid, followed by several trap–to–trap distillations between 273 K and 77 K. The principal impurities in the dehydrated nitric acid were NO_2 and H_2O. The purified nitric acid was stored at 273 K in a light-protected dewar to prevent photolytic decomposition, and was never retained for more than 24 h after the final distillation. All test gas mixtures were prepared using a partial pressure technique in a 2.3 liter Teflon-coated mixing tank with a magnetic stirrer.

A passivation process was utilized to control wall-adsorption effects in the shock tube. The passivation technique consisted of an initial conditioning of the test section of the shock tube with approximately 11 torr of 0.5% HNO_3 in argon. The wall adsorption sites were occupied by the HNO_3 in the passivation mixture, and the shock tube was evacuated to 100 millitorr after approximately 5 min. The test gas mixture was then introduced into the driven section and the experiment was conducted after another 5 min interval. The delay between the final filling and the experiment was necessary to insure spatial uniformity of the test gas mixture in the shock tube. Measured yields of OH indicated that the passivation procedure produced consistent initial HNO_3 concentrations between 0.5 and 1.5 times that in the original mixing tank mixture.

The diagnostic system consisted of a Spectra-Physics 380A cw ring dye laser operated on Rhodamine 590 laser dye and pumped by a Spectra-Physics 164 argon ion laser (4 W, all lines visible). The visible wavelength output of the ring dye laser cavity was monitored by a Burleigh WA-10 wavemeter, and the laser mode quality was monitored by a Spectra-Physics 470 scanning interferometer (2 GHz free spectral range). The fundamental laser frequency was intracavity doubled to the uv by a temperature-controlled AD*A crystal, and the laser was operated with the galvo tuning rhomb assembly in place. Wavelength control was improved by conducting a manual scan across the absorption lineshape in a reference flame of methane and air. The wavelength was centered at the peak absorption of the $R_1(5)$ line prior to each experiment. The uv beam passed through the shock tube perpendicular to the shock tube axis through calcium fluoride windows. The beam intensity was measured before and after passing through the shock tube via fast uv photodiode detectors (EG&G UV100BQ, electronic 3-dB bandwidth of 350 kHz) with a 2.5 mm diameter active surface area. The incident (I_0) and differenced (I_0-I) laser intensities were recorded on a Nicolet 2090 digital oscilloscope using a 0.5 μs sampling rate. The noise on the differenced signal was typically 0.1% of the incident signal, corresponding to a detectivity limit of approximately 1 ppm at $T = 1400$ K, $P = 0.3$ atm, and a path length of 15.24 cm.

Results

OH Absorption Measurements

Figure 2 shows a typical high-temperature OH mol fraction profile. The experimental conditions corresponding to Figure 2 are $T = 2352$ K, $P = 0.196$ atm, and $HNO_3^\circ = 1020$ ppm, where HNO_3° is the initial concentration of nitric acid in the shock tube at the time of the experiment. The absorption data were converted to mol

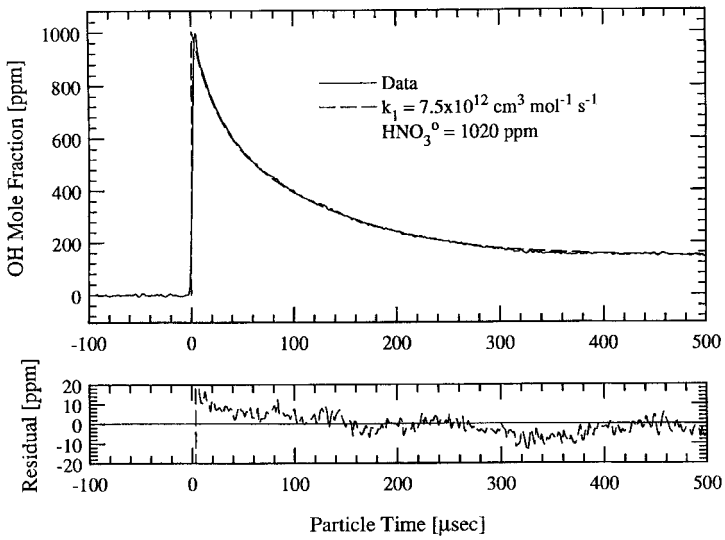

Figure 2. Comparison of experimental and Chemkin-calculated OH profiles using best-fit $k_1 = 7.5 \times 10^{12}$ cm^3 mol^{-1} s^{-1} and $HNO_3^o = 1020$ ppm (incident shock, $T = 2352$ K, $P = 0.196$ atm).

fraction data by applying Beer's law for a narrowline radiation source:

$$I/I_0 = \exp(-k_\nu P \chi_{OH} L)$$

Here, I and I_0 are the transmitted and incident radiation intensities, respectively, k_ν is the spectral absorption coefficient [cm^{-1} atm^{-1}], P is the total pressure [atm], χ_{OH} is the mol fraction of OH, and L is the path length through the absorbing medium [cm]. The absorption coefficient was calculated via

$$k_\nu[\text{cm}^{-1}\ \text{atm}^{-1}] = S(T)\phi(\nu),$$

where $S(T)$ [cm^{-2} atm^{-1}] is the integrated line strength and $\phi(\nu)$ [cm] is the line shape function. The following empirical expression for k_ν was determined using the known line position [3], Einstein coefficient [3], and pressure broadening coefficient [4]

$$k_\nu[\text{cm}^{-1}\ \text{atm}^{-1}] = 18.1 - 2.11 \times 10^5/T + 9.77 \times 10^8/T^2 - 4.06 \times 10^{11}/T^3,$$

and is accurate to 1.2% throughout the temperature range of 1050–2380 K. The relation for k_ν is valid for the linecenter of the $R_1(5)$ $A^2\sum^+ \leftarrow X^2\prod_i (0,0)$ transition with broadening by argon only, at a pressure of 1 atm. The value for k_ν at other pressures can be determined by multiplying the above result by the ratio of the appropriate Voigt functions. The uncertainty in k_ν for the conditions of this investigation is $\pm 5\%$, set primarily by uncertainty in the oscillator strength for this transition.

The mol fraction data were converted from laboratory time (t_1) to particle time (t_p) using the relation $t_p = (\rho_2/\rho_1)t_1$, where ρ_1 is the initial density of the test gas mixture and ρ_2 is the density of the test gas mixture behind the incident shock wave.

All experiments were modeled using the Chemkin-II [5] chemical kinetics simulation package and the Chemkin thermodynamic data base [6]. The reaction mechanism employed is shown in Table I. This 17-reaction mechanism was developed from

TABLE I. Reaction mechanism; rate coefficients in the form $k = AT^{\beta} \exp(-E_A/RT)$ (Units are mol, cc, s, K, and cal).

	Reaction	A	β	E_A	Ref.
⇒	1. $OH + OH = H_2O + O$	9.40×10^{-5}	4.77	−9081.	[a]
⇒	2. $HNO_3 + M = OH + NO_2 + M$	1.01×10^{16}	0.0	34335.	[7]
	3. $HNO_3 + OH = H_2O + NO_3$	9.50×10^{10}	0.0	0.	[21]
⇒	4. $H + O_2 = OH + O$	9.33×10^{13}	0.0	14800.	[22]
	5. $H + OH + M = H_2O + M$	1.60×10^{22}	−2.0	0.	[23]
	Enhanced efficiency for $H_2O \times 5.0$				
	6. $OH + H_2 = H_2O + H$	1.17×10^{9}	1.3	3626.	[23]
	7. $H_2 + O = OH + H$	5.06×10^{4}	2.67	6290.	[23]
	8. $O + HO_2 = O_2 + OH$	1.40×10^{13}	0.0	1073.	[23]
	9. $H + HO_2 = OH + OH$	1.40×10^{14}	0.0	1073.	[23]
⇒	10. $OH + HO_2 = H_2O + O_2$	7.50×10^{12}	0.0	0.	[23]
	11. $H + O_2 + M = HO_2 + M$	3.61×10^{17}	−0.72	0.	[23]
	Enhanced efficiency for $H_2O \times 18.6$				
⇒	12. $NO_2 + H = NO + OH$	3.47×10^{14}	0.0	1470.	[24]
⇒	13. $HO_2 + NO = NO_2 + OH$	2.11×10^{12}	0.0	−479.	[23]
⇒	14. $NO_2 + M = NO + O + M$	1.10×10^{16}	0.0	65571.	[24]
	15. $NO + N = N_2 + O$	4.29×10^{13}	0.0	1564.	[25]
	16. $NO + O = N + O_2$	3.80×10^{9}	1.0	41369.	[24]
	17. $NO_2 + O = NO + O_2$	1.00×10^{13}	0.0	596.	[24]

⇒ Reactions important in this study.
[a]This work.

a more comprehensive 82-reaction model using sensitivity and contribution factor analyses to eliminate reactions that were unimportant for the conditions of the present study. The expression for k_2 is from Wooldridge et al. [7] and was derived from a combination of present low-temperature data ($T < 1400$ K) as well as additional HNO_3 decomposition experiments conducted at lower temperatures. Table II lists the heats of formation at 298 K for the pertinent species.

The high-temperature data were analyzed by adjusting the rate coefficient of reaction (1) and the initial amount of HNO_3 present in the model, and then comparing the calculated OH profiles with the experimental traces. The determination of the best

TABLE II. Heats of formation used in the thermodynamic data base.

Species	ΔH_f° (298 K) [kcal/mol]
OH	9.32
HO_2	2.50
H_2O	−57.80
HNO_3	−32.10
NO_2	7.91
NO	21.58
O	59.55
H	52.09
NO_3	17.00
N_2O	19.61

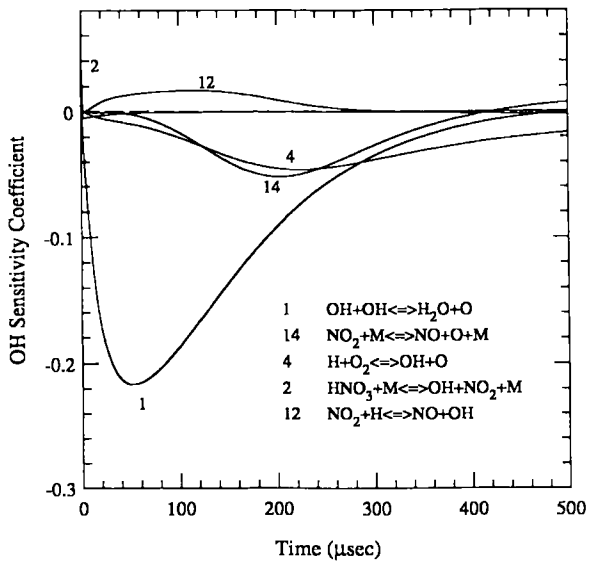

Figure 3. OH sensitivity plot for conditions of Figure 2. The sensitivity coefficient α_{ij} is defined as the partial derivative of the species mol fraction χ_j with respect to the rate constant parameter A_i, normalized by the maximum species mol fraction χ_j^{max} and the rate constant parameter A_i: $\alpha_{ij} = (A_i/\chi_j^{max})(\partial\chi_j/\partial A_i)$.

fit to the experimental profile was aided by the residual trace shown at the bottom of Figure 2. The residual was generated by subtracting the calculated profile from the experimental data trace. The optimum values for k_1 and HNO_3° were obtained by minimizing this residual. Figures 3 and 4 show the OH sensitivity and contribution factor analyses for the conditions of Figure 2, as generated by the Senkin [8] modeling

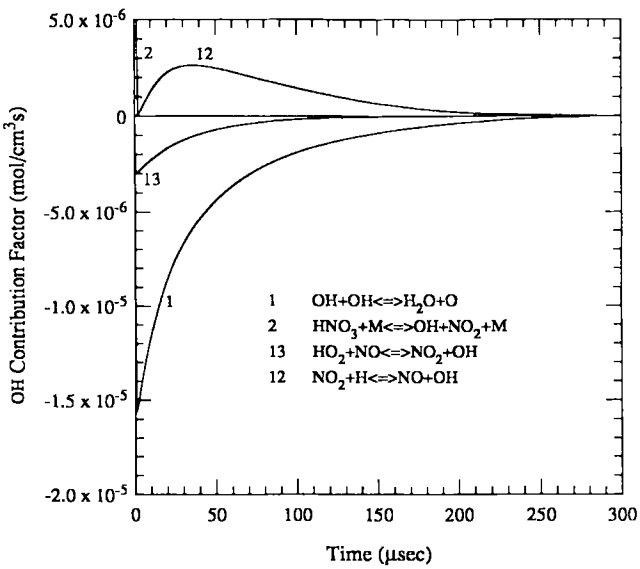

Figure 4. OH contribution plot for conditions of Figure 2.

package. The sensitivity coefficient for a particular species α_{ij} is defined as the partial derivative of the species mol fraction χ_j with respect to the rate constant parameter A_i, normalized by the maximum species mol fraction χ_j^{max} and the rate constant parameter A_i:

$$\alpha_{ij} = (A_i/\chi_j^{max})(\partial\chi_j/\partial A_i)$$

The contribution factor is the rate of production or removal of a species by a particular reaction. The sensitivity and contribution factor analyses indicate that, at high-temperatures, reaction (1) is the dominant reaction affecting the OH profile for times up to ca. 100 μs.

A typical low-temperature OH mol fraction profile is shown in Figure 5. The experimental conditions of this trace are T = 1198 K, P = 0.421 atm, and HNO_3° = 283 ppm. The spike at time-zero (t_0) on the data trace is a consequence of beam-steering as the shock wave passes the diagnostic port. OH is formed by HNO_3 decomposition and is subsequently removed by reaction (1). For the low-temperature OH profiles, the initial portion of the data trace was fit by adjusting the rate coefficient of reaction (2) and the initial amount of HNO_3 present. The latter portion of the profile, where the OH + OH reaction is dominant, was then fit by adjusting the rate coefficient of reaction (1). Residuals were again used to determine the optimum fit-parameters. Figures 6 and 7 show the OH sensitivity and contribution factor analyses for the conditions of Figure 5.

Table III summarizes the shock conditions and the resulting values determined for k_1. The experiments span a temperature range of 1050–2380 K and a pressure range of 0.18–0.60 atm. The data are plotted in Figure 8 and fit by the following expression (of the form $A\ T^\beta \exp(C/T)$) for the rate coefficient of the bimolecular reaction:

$$k_1 = 9.40 \times 10^{-5}\ T^{4.77} \exp(+4570/T\ [\mathrm{K}])\ [\mathrm{cm^3\ mol^{-1}\ s^{-1}}]$$

The standard deviation for this expression is 7%.

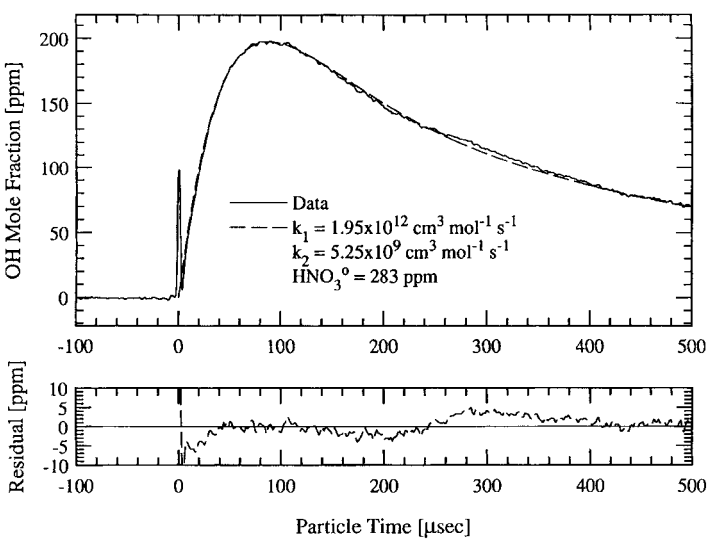

Figure 5. Comparison of experimental and Chemkin-calculated OH profiles using best-fit $k_1 = 1.95 \times 10^{12}$ cm^3 mol^{-1} s^{-1}, $k_2 = 5.25 \times 10^9$ cm^3 mol^{-1} s^{-1} and HNO_3° = 283 ppm (incident shock, T = 1198 K, P = 0.421 atm).

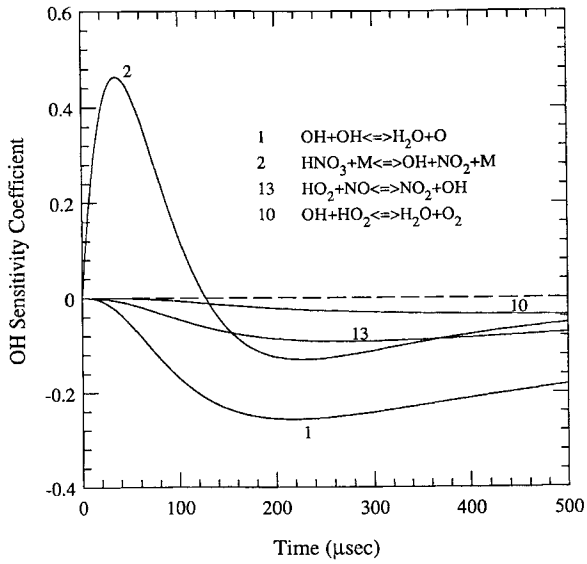

Figure 6. OH sensitivity plot for conditions of Figure 5.

Uncertainty Analysis

An uncertainty analysis was performed using dependent and independent error propagation analysis [9]. This process groups dependent sources of error together as one net source of uncertainty. Each of the independent parameters or groups is then perturbed to its extreme value and the data trace is then reanalyzed. For example, a data trace from the high-temperature regime is reevaluated using the allowed limiting values for the OH spectral absorption coefficient, and new values for k_1 and HNO_3° are determined. For a data trace from the low-temperature regime, a new pair of

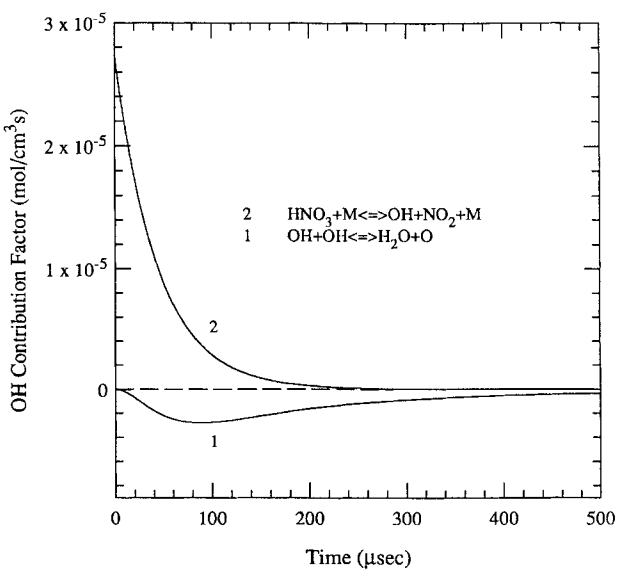

Figure 7. OH contribution plot for conditions of Figure 5.

TABLE III. Experimental conditions and results.

T_2 K	P_2 atm	HNO_3° ppm	k_1 10^{12} cm^3 mol^{-1} s^{-1}
1050	0.217	640	1.95
1069	0.215	374	1.85
1103	0.205	583	1.70
1105	0.365	590	1.85
1118	0.205	717	2.15
1183	0.202	714	2.00
1198	0.421	283	1.95
1228	0.219	562	2.35
1248	0.182	640	2.20
1256	0.183	709	2.40
1300	0.439	342	2.01
1398	0.305	545	2.45
1416	0.405	390	2.55
1494	0.397	625	2.66
1591	0.363	533	2.95
1592	0.364	502	3.10
1644	0.602	232	3.10
1650	0.340	595	3.35
1684	0.253	650	3.65
1750	0.227	868	3.85
1861	0.287	488	4.95
1902	0.292	627	4.75
2013	0.322	430	4.72
2189	0.217	1100	6.40
2265	0.286	1020	7.32
2352	0.196	1020	7.50
2384	0.182	1470	8.56

values for k_2 and HNO_3° are determined to fit the early region of the trace, and then a new value for k_1 is determined to fit the latter region of the trace. Table IV summarizes the results of the uncertainty analysis. As indicated, different sources of uncertainty dominate in different temperature regions. The effects of impurities in the test gas mixture, uncertainty in shock speed measurement, boundary layer effects, and uncertainty in other rate coefficients were found to have negligible impact on the determination for k_1 throughout the temperature range.

The total uncertainty in the rate coefficient of reaction (1) for each of the temperature extremes is determined by combining the effects of each of the independent sources of uncertainty through the relation

$$\text{Total Uncertainty} = \left(\sum(\text{uncertainty})^2\right)^{1/2}$$

An overall uncertainty of +25% −22% is assigned to the low-temperature data, while an overall uncertainty of +11% −16% is assigned to the high-temperature data.

Discussion

Figure 8 is an Arrhenius diagram of the rate coefficients determined in the current work and from other high-temperature studies of k_1 and k_{-1}. There have been only

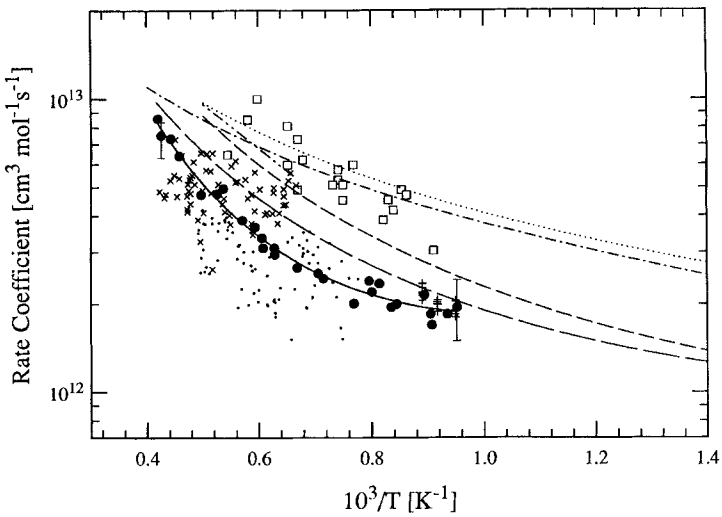

Figure 8. Arrhenius plot of rate coefficients for reaction (1), OH + OH → H_2O + O, determined from the present experiments. Also shown are results from other recent determinations of k_1 and k_{-1}, theoretical models and rate coefficient evaluations. The solid line is a three-parameter fit to the present work, where $k_1 = 9.4 \times 10^{-5}\ T^{4.77}\ \exp(+4570/T\ [\mathrm{K}])$ [cm^3 mol^{-1} s^{-1}]. The vertical error bars are the overall uncertainties determined for the present work. (●) Current work; (□) Ernst et al. (1977); (- - - - -) Rawlins and Gardiner (1974); (— — —) Baulch et al. (1992); (— — —) Harding and Wagner (1989); (----------) Tsang and Hampson (1986); and (——) Michael (1992). Experimental investigations of the reverse reaction: (×) Lifshitz and Michael (1991); (•) and (+) Sutherland et al. (1991).

TABLE IV. Uncertainty analysis for reaction (1): OH + OH → H_2O + O.

Parameter	Uncertainty	Effect on k_1	
Dominant Sources of Uncertainty at High Temperatures: (T > 2100 K)			
OH abs. coeff.	+5%	+4%	
	−5%		−7%
k_{14}	+100%		−13%
	−100%	+9%	
t_o	+3 μs	+4%	
	−3 μs		−5%
Total Uncertainty = $[\sum(\text{uncert.})^2]^{0.5}$:		+11%	−16%
Dominant Sources of Uncertainty at Low Temperatures:			
OH abs. coeff.	+5%	+13%	
	−5%		−8%
k_2, HNO_3°	+20%	+20%	
	−20%		−21%
$\Delta H_f^\circ(298\ \mathrm{K})_{HO_2}$	+0.5 kcal/mol	+7%	
Total Uncertainty = $[\sum(\text{uncert.})^2]^{0.5}$:		+25%	−22%

two other direct studies of reaction (1), both of which yielded rates approximately twice that found in the current work. In an experiment similar to the current study, Ernst, Wagner, and Zellner [10] used nitric acid as a source for OH, but a microwave discharge lamp of H_2O and argon was used in the OH uv absorption measurements. They reported difficulties calibrating their diagnostic and ultimately concluded that "because of insufficient detection sensitivity for OH, however, the HNO_3 source can hardly be recommended for the study of other OH reactions." Gardiner et al. [11] monitored OH profiles in H_2/O_2 mixtures using a Bi lamp as the uv source for OH absorption. Interpretation of their OH profiles required kinetic modeling in order to extract k_1. Their results have been reanalyzed [12] in order to account for changing values of the rate parameters of other reactions.

There have been two recent studies of the reverse reaction,

$$(-1) \qquad H_2O + O \longrightarrow OH + OH$$

Sutherland et al. [13] used a shock tube and flash photolysis of $NO/H_2O/Ar$ mixtures, as well as resonance fluorescence in a flow reactor, to determine k_{-1}. They monitored O-atom profiles via atomic resonance absorption spectroscopy. Although their data display considerable scatter (see Fig. 8), the magnitude and general temperature dependence of the rate coefficient agree well with our findings. Lifshitz and Michael [14] used the same shock tube-flash photolysis technique, as well as dissociation of N_2O as a thermal source of O-atoms, and O-atom absorption to study k_{-1}. They do not report values for k_1, and consequently their data have been converted using the equilibrium constant derived from the JANAF thermodynamic data base. The values for k_1 are shown in Figure 8. The results of Lifshitz and Michael also display a significant degree of scatter, but agree well with the general magnitude of the present data.

There have been several theoretical investigations of reaction (1). Harding and Wagner [15] used variational transition state theory to calculate the rate of reaction (1), and then scaled their results to match room temperature data. Michael [16] used the Harding and Wagner model to derive new relations for k_1 and k_{-1} using conventional transition state theory with Wigner tunneling. The present rate coefficient determination is approximately 0.6 that given by Harding and Wagner and approximately 0.8 that of Michael. The recommendations of Tsang and Hampson [17] and Baulch et al. [18] are included in Figures 8 and 9 for reference.

Figure 9 presents an Arrhenius diagram for reaction (1) including lower temperature data. Wagner and Zellner [19] provide the only experimental results in the intermediate temperature range. They used flash photolysis of N_2 and H_2O in a reaction cell, and monitored the OH time-histories using OH resonance absorption spectroscopy. If the Wagner and Zellner results are taken in conjunction with the present work along with a consensus value for k_1 at $T = 298$ K [20], the following fit to the rate coefficient of reaction (1) is determined for the temperature range 298 K–2380 K

$$k_1 = 3.57 \times 10^4\, T^{2.40} \exp(+1063/T\ [\mathrm{K}])[\mathrm{cm}^3\ \mathrm{mol}^{-1}\ \mathrm{s}^{-1}].$$

The standard deviation for this result is 12.6%. This rate coefficient expression also agrees well with the flash photolysis-resonance fluorescence data of Sutherland et al. [13].

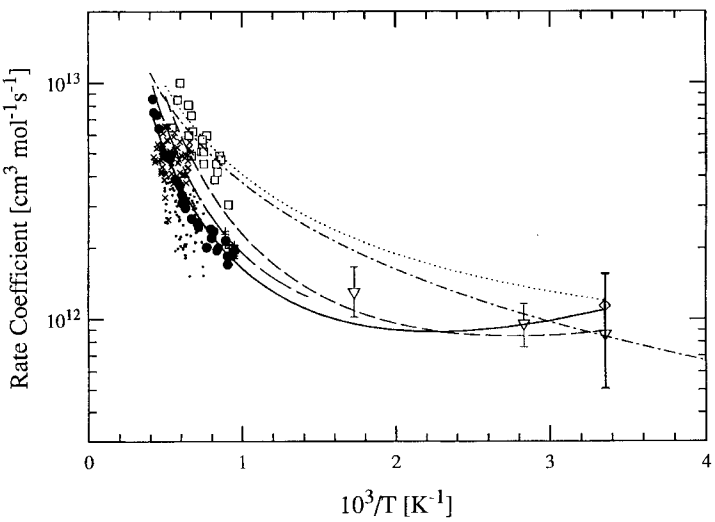

Figure 9. Arrhenius plot of rate coefficients for reaction (1). The solid line is a fit to the present work, the low-temperature data of Wagner and Zellner [19] and a consensus value for k_1 at $T = 298$ K [20], where $k_1 = 3.57 \times 10^4\ T^{2.40}\ \exp(+1063/T\ [\mathrm{K}])[\mathrm{cm}^3\ \mathrm{mol}^{-1}\ \mathrm{s}^{-1}]$. The bold vertical error bar at room temperature indicates the range of values for k_1. The remaining vertical error bars are the uncertainties for the Wagner and Zellner data. (●) Current work; (□) Ernst et al. (1977); (▽) Wagner and Zellner (1981); (◇) NASA (1985); (– – –) Harding and Wagner (1989); (----------) Tsang and Hampson (1986); (– – – –) Baulch et al. (1992); and (——) Michael (1992). Experimental investigations of the reverse reaction: (×) Lifshitz and Michael (1991); (•) and (+) Sutherland et al. (1991).

Conclusions

The rate coefficient for OH + OH → H_2O + O has been measured via narrow-linewidth uv laser absorption of OH. A fit to the data yields the following empirical three-parameter expression valid in the temperature range 1050 K–2380 K

$$k_1 = 9.40 \times 10^{-5}\ T^{4.77}\ \exp(+4570/T\ [\mathrm{K}])[\mathrm{cm}^3\ \mathrm{mol}^{-1}\ \mathrm{s}^{-1}]$$

with an overall uncertainty ranging from +11%, −16% at high temperatures to +25%, −22% at low temperatures.

Incorporating the low-temperature data of Wagner and Zellner [19] and a consensus value for k_1 at $T = 298$ K [20], the following empirical fit is determined for the temperature range 298 K–2380 K:

$$k_1 = 3.57 \times 10^4\ T^{2.40}\ \exp(+1063/T\ [\mathrm{K}])[\mathrm{cm}^3\ \mathrm{mol}^{-1}\ \mathrm{s}^{-1}].$$

The results of the current study are in good agreement with recent studies by Sutherland et al. [13] and Lifshitz and Michael [14] of the reverse reaction, but are lower than the rate coefficient expressions recommended by Baulch et al. [18], Tsang and Hampson [17], and Harding and Wagner [15]. The scatter of the current data, however, is significantly reduced relative to other high-temperature studies.

Acknowledgment

This work was supported by the U. S. Environmental Protection Agency and the National Science Foundation. We would like to thank Steven T. Wooldridge, David F. Davidson, and Michael D. Di Rosa for assistance in the laboratory and helpful comments.

Bibliography

[1] J. Warnatz, *Twenty-Fourth Symposium (International) on Combustion,* The Combustion Institute, Pittsburgh, 553, 1992.
[2] S. A. Stern, J. T. Mullhaupt, and W. B. Kay, *Chem. Rev.,* **60,** 185 (1960).
[3] A. Goldman and J. R. Gillis, *J. Quant. Spectrosc. Rad. Transfer,* **25,** 111 (1981).
[4] E. C. Rea, Jr., A. Y. Chang, and R. K. Hanson, *J. Quant. Spectrosc. Rad. Transfer,* **37,** 117 (1987).
[5] R. J. Kee, F. M. Rupley, and J. A. Miller, *Chemkin-II: A Fortran Chemical Kinetics Package for the Analysis of Gas-Phase Chemical Kinetics,* Report No. SAND89-8009, Sandia National Laboratories, Livermore, California, 1989.
[6] R. J. Kee, F. M. Rupley, and J. A. Miller, *The Chemkin Thermodynamic Data Base,* Report No. SAND87-8215B, Sandia National Laboratories, Livermore, California, 1990.
[7] M. S. Wooldridge, R. K. Hanson, and C. T. Bowman, *Shock Waves: Proceedings of the Nineteenth International Symposium on Shock Waves,* Springer-Verlag, Berlin, 1994.
[8] A. E. Lutz, R. J. Kee, and J. A. Miller, *SENKIN: A Fortran Program for Predicting Homogeneous Gas-Phase Chemical Kinetics with Sensitivity Analysis,* Report No. SAND87-8248, Sandia National Laboratories, Livermore, California, 1988.
[9] S. L. Meyer, *Data Analysis for Scientists and Engineers,* Wiley, New York, 1975.
[10] J. Ernst, H. Gg. Wagner, and R. Zellner, *Ber. Bunsenges. Phys. Chem.,* **81,** 1270 (1977).
[11] W. C. Gardiner, Jr., K. Morinaga, D. L. Ripley, and T. Takeyama, *J. Chem. Phys.,* **48,** 1665 (1968).
[12] W. T. Rawlins and W. C. Gardiner, Jr., *J. Chem. Phys.,* **60,** 4676 (1974).
[13] J. W. Sutherland, P. M. Patterson, and R. B. Klemm, *Twenty-Third Symposium (International) on Combustion,* The Combustion Institute, Pittsburgh, 51, 1991.
[14] A. Lifshitz and J. V. Michael, *Twenty-Third Symposium (International) on Combustion,* The Combustion Institute, Pittsburgh, 59, 1991.
[15] L. B. Harding and A. F. Wagner, *Twenty-Second Symposium (International) on Combustion,* The Combustion Institute, Pittsburgh, 983, 1989.
[16] J. V. Michael, *Prog. Energy Comb. Sci.,* **18,** 327 (1992).
[17] W. Tsang and R. F. Hampson, *J. Phys. Chem. Ref. Data,* **15,** 1087 (1986).
[18] D. L. Baulch, C. J. Cobos, R. A. Cox, C. Esser, P. Frank, Th. Just, J. A. Kerr, M. J. Pilling, J. Troe, R. W. Walker, and J. Warnatz, *J. Phys. Chem. Ref. Data,* **21,** 411 (1992).
[19] G. Wagner and R. Zellner, *Ber. Bunsenges. Phys. Chem.,* **85,** 1122 (1981).
[20] NASA, *Chemical Kinetics and Photochemical Data for Use in Stratospheric Modeling,* Evaluation No. 7, NASA Panel for Data Evaluation, JPL Publication 85–37, 1985.
[21] K. Glänzer and J. Troe, *Ber. Bunsenges. Phys. Chem.,* **78,** 71 (1974).
[22] D. A. Masten, R. K. Hanson, and C. T. Bowman, *J. Phys. Chem.,* **94,** 7119 (1990).
[23] J. A. Miller and C. T. Bowman, *Prog. Energy. Comb. Sci.,* **15,** 287 (1989).
[24] R. K. Hanson and S. Salimian, In *Combustion Chemistry,* W. C. Gardiner, Jr., Ed., Springer-Verlag, New York, 361, 1984.
[25] D. F. Davidson and R. K. Hanson, *Int. J. Chem. Kinet.,* **22,** 843 (1990).

Received April 19, 1993
Accepted July 26, 1993